Analytic model of electron self-injection in a plasma wakefield accelerator in the strongly nonlinear bubble regime

S. A. Yi, V. Khudik, C. Siemon, and G. Shvets

Citation: AIP Conference Proceedings **1507**, 410 (2012); doi: 10.1063/1.4773731

View online: http://dx.doi.org/10.1063/1.4773731

View Table of Contents: http://scitation.aip.org/content/aip/proceeding/aipcp/1507?ver=pdfcov

Published by the AIP Publishing

Analytic model of electron self-injection in a plasma wakefield accelerator in the strongly nonlinear bubble regime

S. A. Yi, V. Khudik, C. Siemon and G. Shvets

The Department of Physics and Institute for Fusion Studies, The University of Texas at Austin, One University Station C1500, Austin, Texas

Abstract. Self-injection of background electrons in plasma wakefield accelerators in the highly nonlinear bubble regime is analyzed using particle-in-cell and semi-analytic modeling. It is shown that the return current in the bubble sheath layer is crucial for accurate determination of the trapped particle trajectories.

Keywords: plasma wakefield accelerators; self injection
PACS: 52.40.Mj, 52.59.-f, 52.59.Bi, 52.59.Fn, 52.65.Rr

INTRODUCTION

Electron beam driven plasma wakefield accelerators (PWFA) have attracted interest for their ability to substantially boost the maximum electron energy of existing accelerator facilities [1]. Such schemes aim to efficiently transfer energy from an electron drive bunch to a witness bunch using a plasma wave as the intermediary. A plasma "afterburner", operated in the highly nonlinear bubble regime [2, 3] is able to take advantage of extremely high accelerating gradients, constant longitudinal accelerating fields [4], and focusing transverse fields. In the bubble regime self-injection may also occur, whereby background plasma electrons initially at rest become trapped inside bubble and become accelerated.

Injection can originate from a variety of mechanisms, such as bubble expansion [5, 6] or field ionization [7]. In the case of laser driven wakefield acceleration, self-injection is often desirable, because no external injectors are required, and may occur naturally due to the nonlinear evolution of the laser pulse and the associated bubble expansion. For PWFA afterburners, self-injection should be avoided, since self-injected electrons produce "dark current" of lower energy than the witness bunch. Since density downramps cause bubble expansion, the background density inhomogeneities that can lead to injection must be understood to prevent dark current formation.

In this paper, we analyze self-injection into a PWFA, where bubble expansion is due to density inhomogeneities. First, we briefly describe an analytic model of the beam driven bubble, leaving the details of the derivation to a longer paper [8]. This analytic model extends previous work [9, 10] for bubble fields inside the bubble to give globally applicable expressions for the wakefields in the bubble exterior and interior. Next, we use the new model to calculate the trajectory of initially quiescent plasma electrons that interact with the ultrarelativistic bubble, and show that accurate analytic description of the return current surrounding the bubble is required for self-injection studies. Finally, we analyze within a Hamiltonian framework [5, 6] the self-injection of electrons due to their interaction with the deepening potential well of a growing bubble.

ANALYTIC MODEL OF BUBBLE STRUCTURE

The quasi-static approximation

We begin by defining several key dimensionless variables by normalized units, where time is normalized to ω_p^{-1}, length to $k_p^{-1} = c/\omega_p$, charge and mass to the electron charge e and electron mass m, respectively, density to n_0, current density to ecn_0, and potential to mc^2/e. Here $\omega_p^2 \equiv 4\pi e^2 n_0/m$, where n_0 is the background plasma density. Maxwell's

Advanced Accelerator Concepts
AIP Conf. Proc. 1507, 410-415 (2012); doi: 10.1063/1.4773731

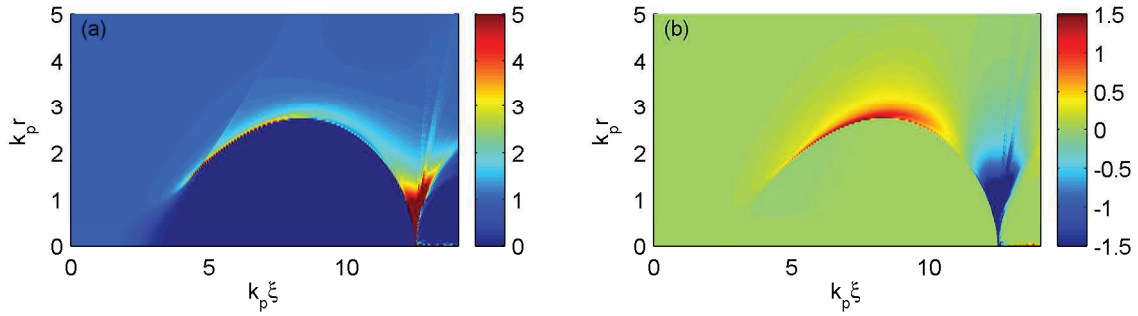

FIGURE 1. (a): Plasma electron density and (b): return current density from PIC simulation. Note that the color scales in each subfigure are capped at different levels due to the large difference in the peak magnitude of the two quantities, i.e., $max(\rho_{elec}) \gg max(J_{z,elec})$. For simplicity, the contributions from the electron beam driver are not shown.

equations in the Lorenz gauge for the potentials are

$$\left(\frac{\partial^2}{\partial t^2} - \nabla^2\right) \left[\begin{array}{c} \mathbf{A} \\ \phi \end{array} \right] = \left[\begin{array}{c} \mathbf{J} \\ \rho \end{array} \right], \tag{1}$$

where we have normalized the current and charge densities to ecn_0 and en_0 respectively. Transforming to the co-moving variables $(t, \xi \equiv t - z)$ and applying the quasi-static approximation [11] $\partial_t \ll \partial_\xi$, we obtain the following simplification of Maxwell's equations [12, 13]:

$$-\nabla_\perp^2 \left[\begin{array}{c} \mathbf{A} \\ \phi \end{array} \right] = \left[\begin{array}{c} \mathbf{J} \\ \rho \end{array} \right]. \tag{2}$$

Here, the Lorenz gauge condition is given by $\nabla_\perp \cdot \mathbf{A}_\perp = -\partial\psi/\partial\xi$, where we have defined the pseudopotential $\psi \equiv \phi - A_z$. From cylindrical symmetry $\mathbf{A}_\perp = A_r \hat{r}$, and the gauge condition allows A_r to be computed from ψ. Thus, when the source terms ρ and J_z are known, ψ and A_z can be calculated by solving Eq. (2). From the potentials all non-vanishing fields can be obtained according to the following expressions:

$$E_z = \frac{\partial\psi}{\partial\xi}, \qquad E_r = -\frac{\partial\phi}{\partial r} - \frac{\partial A_r}{\partial\xi}, \qquad B_\theta = -\frac{\partial A_r}{\partial\xi} - \frac{\partial A_z}{\partial r}. \tag{3}$$

Below we introduce a simple model for the source terms in Eq. (2) for both inside and outside the bubble. The source terms for charge density are comprised of that of the beam, surrounding plasma and stationary ions, respectively given by ρ_{beam}, ρ_{elec} and ρ_{ion}. The current is composed of the beam and plasma current densities, $J_{z,beam}$ and $J_{z,elec}$, respectively.

Source terms

The density profile for the electron beam driver is defined as

$$\rho_b(\xi, r) \equiv J_{z,beam}/c = \frac{N}{(2\pi)^{3/2}\sigma_r^2\sigma_z} \exp\left(\frac{-r^2}{2\sigma_r^2} + \frac{-\xi^2}{2\sigma_z^2}\right),$$

where N is the number of beam electrons, and $\sigma_{r,z}$ are the transverse and longitudinal widths of the beam, respectively. We are considering the case of a highly relativistic (i.e., very rigid) driver, so that drive beam evolution is negligible. We further take ions to be immobile, i.e., $\rho_{ion} = en_0$. The total charge density is then $\rho = \rho_{beam} + \rho_{elec} + \rho_{ion}$, and the total longitudinal current is $J_z = J_{z,beam} + J_{z,elec}$.

Next, we assume a current and density distribution profile of the plasma electrons which will fully specify the source terms in Eq. (2). The drive beam causes complete cavitation of plasma electrons inside the bubble, so that the

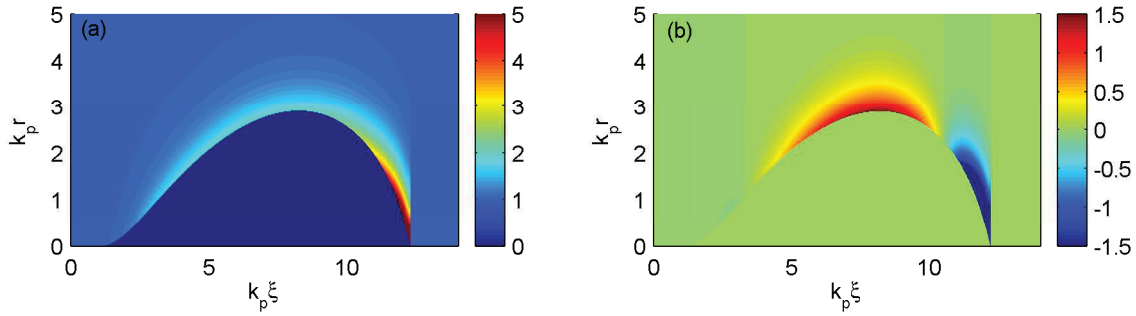

FIGURE 2. (a): Plasma electron density and (b): return current density $J_s(\xi)e^{-(r-r_b)/\Delta_J}\theta(r-r_b)$ from the analytic model, Eq. (8). For simplicity, the contributions from the electron beam driver are not shown.

bubble contains only ions, i.e., $\rho_{elec}=0$ inside. This bubble is assumed to have a clearly defined boundary given by the function $r_b(\xi)$, which as demonstrated earlier [9, 10] can be approximated by the trajectory of a single inner-most electron. We assume an exponential dependence $\rho_{elec}\approx\rho_s\exp[-(r-r_b(\xi))/\Delta_\rho]$ for the dense electron sheath layer immediately outside the bubble, so that Δ_ρ can be thought of as the characteristic decay length of the dense plasma density sheath layer. In our model, Δ_ρ does not depend on ξ. Such a density profile is consistent with the plasma density distribution observed in the PIC simulation WAKE [14], as shown in Fig. 1(a). We thus define the source term for Eq. (2) $S(\xi,r)\equiv-(\rho-J_z)$ as

$$S(\xi,r)=\begin{cases}-1 & (r<r_b(\xi)),\\ S_0(\xi)e^{-(r-r_b(\xi))/\Delta_\rho} & (r\geq r_b(\xi)),\end{cases} \tag{4}$$

where $S_0(\xi)$ is the value of the source function $S(\xi,r)$ at $r=r_b(\xi)$. We note that $\rho-J_z\approx\rho$ is observed in PIC simulations consistently, so that the length scale Δ_ρ for the source term $S(\xi,r)$ is taken to be the same as that for the electron density ρ_{elec}. To complete our description of the source terms we also take into account a plasma return current surrounding the outside of the bubble, so that the total longitudinal current is specified as

$$J_z(\xi,r)=J_{z,beam}(\xi,r)+J_s(\xi)e^{-(r-r_b(\xi))/\Delta_J}\theta(r-r_b(\xi)). \tag{5}$$

Here, Δ_J is the width of the sheath return current, $\theta(x)$ is the Heaviside function, and the function $J_s(\xi)$ represents the longitudinal structure of the return current. The existence of such a return current is also consistent with PIC simulation results, as shown in Fig. 1(b). Physically, the return current shields the the displacement current inside the bubble so that the azimuthal magnetic field B_θ vanishes far away at $r\to\infty$. Taking this return current into account is crucial, since the unshielded magnetic field within the return current layer $r_b(\xi)<r<r_b(\xi)+\Delta_J$ plays an important role in determining the trajectories of electrons that stream along the edge of the bubble and become candidates for self-injection. Extension of the magnetic field B_θ to outside the bubble edge is also confirmed in PIC simulations. We have assumed here that the return current also decays exponentially for $r\geq r_b(\xi)$ but has a different thickness Δ_J than $S(\xi,r)$. The introduction of separate length scales for the source terms $\rho-J_z$ and J_z is justified since $\rho-J_z\approx\rho$.

The charge continuity equation $\partial\rho/\partial t+\nabla\cdot J=0$ under the quasi-static approximation can be expressed as [11]

$$\frac{\partial}{\partial\xi}(\rho-J_z)+\frac{1}{r}\frac{\partial}{\partial r}(rJ_r)=0. \tag{6}$$

Since the second term of the above equation clearly vanishes upon integration over the transverse plane it follows that $\partial_\xi\int_0^\infty S(r)rdr=0$ for all values of ξ, which allows us to obtain

$$S_0(\xi)=\frac{r_b^2(\xi)}{2\Delta_\rho(r_b(\xi)+\Delta_\rho)}. \tag{7}$$

For $r\to\infty$, $B_\theta=-(\partial A_z/\partial r+\partial A_r/\partial\xi)=0$ so that $\int_0^\infty(J_z+d^2\psi/d\xi^2)rdr=0$, and it follows that the sheath layer current is given by

$$J_s(\xi)=\frac{\lambda(\xi)-\int_0^\infty rdrd^2\psi/d\xi^2}{\Delta_J(r_b(\xi)+\Delta_J)}. \tag{8}$$

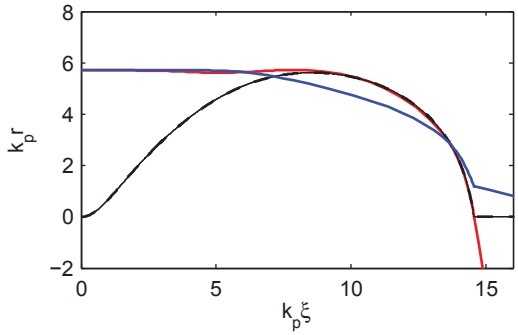

FIGURE 3. Electrons interacting with a non-evolving bubble (solid black) with parameters $\lambda_0 = 6$, $\sigma_z = \sqrt{2}k_p{}^{1}$ and $\Delta_\rho = 0.5k_p{}^{1}$, and with shielded (blue, $\Delta_J = 0.5k_p^{-1}$) and unshielded (red, $\Delta_J = k_p^{-1}$) magnetic field in the return current layer. The electron-bubble interaction length is longer in the unshielded case (red), where the electron follows along the edge of the bubble.

Fig. 2(b) shows a plot of the return current given by Eq. (8), which compares well with that from PIC simulation shown in Fig. 1(b).

The source terms of Eq. (2) have been fully specified by the above assumptions. It follows from the argument in the previous subsection that all bubble fields can now be found. Details on calculation of the wake field quantities, as well as the shape function $r_b(\xi)$ are presented in Ref. [8]. In this paper we will instead concentrate on the trapped electron trajectories calculated using the model fields in the following section.

ELECTRON TRAPPING

Effect of return current on particle trajectories

We now apply the bubble fields given by the model described in the previous section to study the trajectories of initially quiescent plasma electrons that interact with ultra-relativistic bubbles. In order for model electron trajectories to closely match that from PIC simulations it is critical that the return current is thicker than the density sheath, .i.e., $\Delta_J > \Delta_\rho$. This is because the unshielded azimuthal magnetic field B_θ within the sheath layer $r_b(\xi) < r < r_b(\xi) + \Delta_J$ affects the trajectories of electrons that stream close along the bubble boundary. We have found by comparing to PIC simulations that $\Delta_J \approx 2\Delta_\rho$ accurately reproduces the current and charge distributions surrounding the bubble. This is physically reasonable, since the plasma is expected to form a dense electron sheath to shield the positive charge of the bubble on the Debye length scale $\lambda_D \equiv \sqrt{k_B T_e / e^2 n_0}$. On the other hand, the return current layer is spread out over a collisionless skin depth $k_p^{-1} > \lambda_D$, the characteristic length scale of plasma wakes.

Fig. 3 demonstrates the role of the return current in determining the particle trajectories, which shows the trajectory of electrons interacting with a bubble given by the parameters $\lambda_0 = 6$, $\sigma_z = \sqrt{2}$, and $\Delta_\rho = 0.5$. For the blue trajectory $\Delta_J = \Delta_\rho$, so that the sheath magnetic field is shielded and does not play a role. In this case, the electron does not follow along the bubble edge but rather penetrates through the bubble. For the case of the red electron, $\Delta_J = 1 > \Delta_\rho$, and an unshielded B_θ in the sheath layer causes the electrons to stream the bubble edge. We have found that regardless of the electron initial radial offset r_0 (or impact parameter), the bubble-electron interaction length is always longer in the unshielded case ($\Delta_J > \Delta_\rho$. Since the electrons that are the most likely to become trapped are those that interact with the bubble the most strongly, the return current layer and its associated magnetic fields play a critical role in determining the trajectories of trapped electrons. Trapping of initially quiescent plasma electrons by both frozen and growing bubbles will be analyzed in the following subsections.

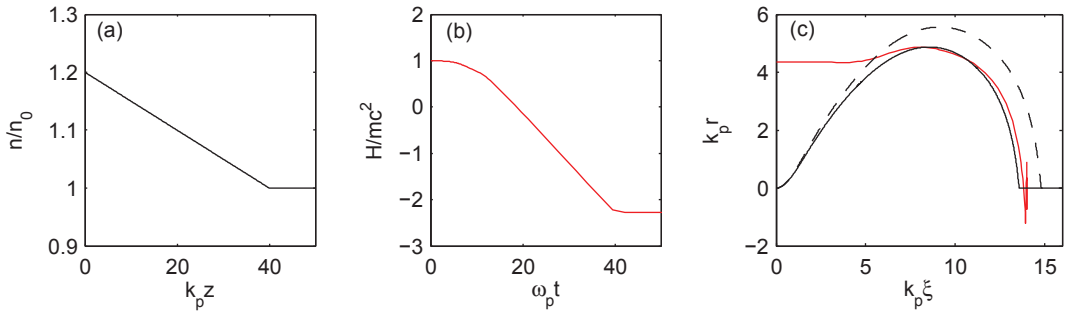

FIGURE 4. Self-injection into an evolving bubble growing due to a density downramp. (a): background plasma density downramp along the propagation distance, z. Here, the downramp is very slow, i.e., $\varepsilon \equiv n^{-1}dn/dz \ll 1$. (b): electron moving-frame Hamiltonian. The electron is trapped once $H < 0$. (c): initial (solid black) and final (dashed black) size of the bubble, and trajectory of an injected electron (red). The parameters here are $\lambda_0 = 6$, $\sigma_z = 1.8k_p^{-1}$, $\Delta_\rho = 0.4k_p^{-1}$, $\Delta_J = k_p^{-1}$, $n_i = 1.2n_0$, $n_f = n_0$, and $L_{\rm ramp} = 40k_p^{-1}$. The initial radial position of the trapped electron is $r_0 = 4.36k_p^{-1}$.

Trapping in a non-evolving bubble

Trapping studies within the context of analytic or semi-analytic models offer the advantage of lower numerical noise and more thorough parameter space scans when compared to PIC simulations. Previous works [15, 16] have shown using a phenomenological non-evolving spherical bubble model that trapping is possible for large enough blowout radii, where the critical blowout radius for trapping scales linearly with the bubble relativistic factor γ_0. Other authors [17] have found empirically (from PIC simulations) that when the radius exceeds several collisionless skip depths trapping always occurs for non-evolving bubbles regardless of the bubble velocity.

Using our model we have performed detailed parameter scans looking for trapping in non-evolving bubbles for a wide range of bubble sizes. We changed the bubble radius by varying the drive beam current λ_0, while the beam length was limited a small range near the resonance $\sigma_z \approx \sqrt{2}$. We further scanned the density sheath width in a small range near $\Delta_\rho \approx 0.5$, while keeping the return current width fixed at $\Delta_J = 1.0$. For normalized bubble radii in the range $3 \sim 12$ we observed no trapping in the case of a non-evolving bubble. We note that in our model the bubble velocity is equal to the speed of light. Thus, in the ultra relativistic limit $v_0 \to c$ we found no evidence of trapping in non-evolving bubbles of normalized radii of order unity. This result is consistent with the conclusions of Refs. [15, 16] since for $\gamma_0 \to \infty$ no trapping is expected for any finite bubble radii. In the next subsection, we move on to explore trapping for the case of evolving bubbles.

Trapping in an expanding bubble

In this section we shift our focus to self-injection of electrons that interact with a a growing bubble. A density downramp enforces bubble evolution, since from force balance the maximum blowout radius can be estimated as

$$r_{bubble}(z) \approx r_{beam}\sqrt{\frac{n_{beam}}{n_{plasma}(z)}}\,. \tag{9}$$

In contrast to Ref. [18] which considered the case of sudden density transitions, we consider here only slow density downramps that cause the bubble to double in size over many bubble lengths, i.e., $\varepsilon \equiv n^{-1}dn/dz \ll 1$.

The trajectory of a plasma electron that becomes trapped and accelerated by a growing bubble is shown as an example in Fig. 4. Here, the model parameters are $\lambda_0 = 6$, $\sigma_z = 1.8$, and $\Delta_\rho = 0.4$. Fig. 4(a) shows the variation of the background plasma density along the propagation distance z, with an initial density $n_i = 1.2\ n_0$ and a linear downramp that reduces the density to $n_f = n_0$ over a distance $L_{\rm ramp} = 40$. The bubble grows as a result of the density downramp as shown in Fig. 4(c): the solid black line is the initial bubble size, and the dashed black line is final bubble size. Such a gradual density gradient would cause this bubble to double in size over several tens of bubble lengths, so that the bubble growth rate is very slow. The trajectory of the trapped electron, which has an impact parameter of $r_0 \approx 4.4$, is

shown in red. Fig. 4(b) shows the Hamiltonian of the trapped electron in the frame co-moving with the bubble,

$$H = \sqrt{1 + (\mathbf{P} + \mathbf{A})^2} - v_0 P_z - \phi \,. \tag{10}$$

Interaction with the deepening potential well of the growing bubble lowers the moving-frame Hamiltonian. Once the trapping condition [5, 6] $H < 0$ is satisfied, the electron cannot leave the well and is accelerated by the bubble.

We have compared model results with those from WAKE simulations, and found that the model agrees quantitatively with WAKE in the bubble growth rate sufficient for electron trapping. This is in contrast to our previous estimates [5, 6] utilizing a simplified spherical bubble model, which overestimated the expansion rate required for trapping. Since the spherical bubble model did not take into account the return current and electromagnetic fields outside the bubble, it is clear that the fields surrounding the bubble must be taken into account in order to properly resolve electron self-injection.

CONCLUSION

We have presented here an analytic model for PWFA in the bubble regime that gives expressions for the fields that are valid globally, and which allows for the study of self-injection. Through this model we have demonstrated that the plasma return current surrounding the bubble and the associated electromagnetic fields play a crucial role in determining the trajectories of trapped electrons. Furthermore, we used this model to study the self-injection phenomenon with an evolving bubble, and confirmed that reduction of the electron moving-frame Hamiltonian to a negative value is a sufficient condition for trapping, in agreement with our previous studies for laser-driven bubbles [5, 6]. In contrast to those past studies which used a spherical bubble model that does not take fields outside the bubble into account, the new model results are in quantitative agreement with PIC simulations.

ACKNOWLEDGMENTS

This work is supported by the US DOE grants DE-FG02-04ER41321 and DE-FG02-07ER54945.

REFERENCES

1. I. Blumenfeld *et al.*, *Nature* **445**, 741 (2007).
2. J. B. Rosenzweig *et al.*, *Phys. Rev. A* **44**, R6189 (1991).
3. A. Pukhov and J. Meyer-ter-Vehn, *Appl. Phys. B* **74**, 355 (2002).
4. M. Tzoufras *et al.*, *Phys. Rev. Lett.* **101**, 145002 (2008).
5. S. Kalmykov *et al.*, *Phys. Rev. Lett.* **103**, 135004 (2009).
6. S. A. Yi *et al.*, *Plasma Phys. Control. Fusion* **53**, 014012 (2011).
7. A. Pak *et al.*, *Phys. Rev. Lett.* **104**, 025003 (2010).
8. S. A. Yi *et al.*, (*In Preparation*, 2012).
9. W. Lu *et al.*, *Phys. Rev. Lett.* **96**, 165002 (2006).
10. W. Lu *et al.*, *Phys. Plasmas* **13**, 056709 (2006).
11. P. Sprangle, *et al.*, *Phys. Rev. Lett.* **64**, 2011 ÍŠ(1990ÍŠ).
12. R. Keinigs *et al.*, *Phys. Fluids* **30**, 252 (1987).
13. D. H. Whittum *et al.*, *Phys. Rev. Lett.* **67**, 991 (1991).
14. P. Mora and T. M. Antonsen, Jr., *Phys. Plasmas* **4**, 217 (1997).
15. I. Kostyukov *et al.*, *Phys. Plasmas* **11**, 5256 (2004).
16. I. Kostyukov *et al.*, *Phys. Rev. Lett.* **103**, 175003 (2009).
17. W. Lu *et al.*, *Phys. Rev. ST - Accel. Beams* **10**, 061301 (2007).
18. H. Suk *et al.*, *Phys. Rev. Lett.* **86**, 1011 (2001).